PHYSICAL REVIEW C **96**, 051303(R) (2017)

Chiral geometry in symmetry-restored states: Chiral doublet bands in ^{128}Cs

F. Q. Chen (陈芳祁),[1] Q. B. Chen (陈启博),[1] Y. A. Luo (罗延安),[2] J. Meng (孟杰),[1,3,*] and S. Q. Zhang (张双全)[1,†]

[1]*State Key Laboratory of Nuclear Physics and Technology, School of Physics, Peking University, Beijing 100871, People's Republic of China*

[2]*School of Physics, Nankai University, Tianjin 300071, People's Republic of China*

[3]*School of Physics and Nuclear Energy Engineering, Beihang University, Beijing 100191, People's Republic of China*

(Received 24 August 2017; published 20 November 2017)

The pairing-plus-quadrupole Hamiltonian is diagonalized in a symmetry-restored basis, i.e., the triaxial quasiparticle states with angular momentum and particle number projections, and applied for chiral doublet bands in ^{128}Cs. The observed energy spectra and electromagnetic transition probabilities are reproduced well without introducing any parameters. The orientation of the angular momentum in the intrinsic frame is investigated by the distributions of its components on the three principle axes (*K plot*) and those of its tilted angles (*azimuthal plot*). The evolution of the chirality with spin is illustrated, and the chiral geometry is demonstrated in the angular momentum projected model for the first time.

DOI: 10.1103/PhysRevC.96.051303

Spontaneous symmetry breaking, in particular spontaneous chiral symmetry breaking, is a subject of general interest. Spontaneous chiral symmetry breaking in atomic nuclei has attracted intensive investigation since its first prediction by Frauendorf and Meng in 1997 [1]. Due to the existence of high-j proton (neutron) particle(s) and neutron (proton) hole(s), the nuclear triaxial shape, and the couplings between single-particle and collective motions, the total nuclear angular momentum vector may lie outside the three principal planes in the intrinsic frame, leading to the spontaneous chiral symmetry breaking. The experimental signal of the spontaneous chiral symmetry breaking is the observation of the chiral doublet bands, which are a pair of nearly degenerate $\Delta I = 1$ bands with the same parity. The evidence of the chiral doublet bands was first observed in 2001 [2]. So far, around 40 candidates of chiral doublet bands have been reported in $A \sim 80$ [3,4], 100 [5–10], 130 [2,11–16], and 190 [17,18] mass regions experimentally, see Refs. [19–21] for reviews. Theoretically, the chiral doublet bands are studied by the particle rotor model (PRM) [1,22–25], the titled axis cranking (TAC) model [1,26–30], the TAC plus random-phase approximation [31], the collective Hamiltonian [32,33], and the interacting boson-fermion-fermion model [12,34,35].

The angular momentum projection (AMP) approach restores the rotational symmetry spontaneously broken in the mean-field approximation and combines the advantages of the TAC model and the PRM. One of the AMP approaches is the projected shell model [36–39], and its applications to triaxial nuclei coupled with quasiparticles can be found in Refs. [40–43]. The attempts to understand the chiral doublet bands by the projected shell model have been performed in Refs. [42,43]. Although the observed energy spectra and transitions have been well reproduced in the AMP approach, a more convincing proof of the chiral picture is to find physical quantities that are linked directly to chiral symmetry. As there is no operator of a physical observable connected directly to the chiral symmetry, the examination of the chiral geometry in the intrinsic frame is what one can best do. However, it is a big challenge to examine the chiral geometry of angular momentum in the AMP approach due to the complication that the projected basis is defined in the laboratory frame and forms a nonorthogonal set.

In this Rapid Communication, the chiral geometry of the angular momentum is investigated within the framework of the AMP approach. The geometry of the angular momentum is analyzed in terms of the distributions of its components on the three intrinsic axes (*K plot*) as well as the distribution of its tilted angles in the intrinsic frame (*azimuthal plot*), which are calculated within the framework of the AMP for the first time. The typical chiral nucleus ^{128}Cs [14] is investigated as an example.

As a starting point, we adopt the standard pairing-plus-quadrupole Hamiltonian [44],

$$\hat{H} = \hat{H}_0 - \frac{\chi}{2}\sum_{\mu=-2}^{2}\hat{Q}^+_\mu\hat{Q}_\mu - G_M\hat{P}^+\hat{P} - G_Q\sum_{\mu=-2}^{2}\hat{P}^+_\mu\hat{P}_\mu, \tag{1}$$

which includes the spherical single-particle Hamiltonian, the quadrupole-quadrupole interaction, as well as the monopole and quadrupole pairing. The intrinsic state $|\Phi\rangle$ is obtained by the constrained calculation,

$$\delta\langle\Phi|\hat{H} - \lambda_n\hat{N} - \lambda_p\hat{Z} - \lambda_{q_0}\hat{Q}_0 - \lambda_{q_2}\hat{Q}_2|\Phi\rangle = 0, \tag{2}$$

with λ_n and λ_p determined by the particle numbers N and Z and λ_{q_0} and λ_{q_2} determined by the quadrupole moments. For odd-odd nucleus, we use $|\Phi_{\nu\pi}\rangle$ to denote the intrinsic state with the neutron (proton) single-particle orbital $\nu(\pi)$ blocked. The space of the intrinsic states is spanned by the states $|\Phi_\kappa\rangle \in \{|\Phi_{\nu\pi}\rangle, |\Phi_{\nu\bar{\pi}}\rangle, |\Phi_{\bar{\nu}\pi}\rangle, |\Phi_{\bar{\nu}\bar{\pi}}\rangle\}$ in which $\bar{\nu},\bar{\pi}$ represent the time-reversal conjugates of ν,π.

The Hamiltonian (1) is diagonalized in the symmetry-restored basis obtained by the projection approach,

$$\left\{\hat{P}^I_{MK}|\Phi_{N,Z,\kappa}\rangle\right\} \equiv \left\{\hat{P}^I_{MK}\hat{P}^N\hat{P}^Z|\Phi_\kappa\rangle\right\}, \tag{3}$$

*mengj@pku.edu.cn
†sqzhang@pku.edu.cn

with the three-dimensional angular momentum projector $\hat{P}^I_{MK}$ and the particle number projectors $\hat{P}^N$ and $\hat{P}^Z$ [44]. The corresponding eigenfunctions are as follows:

$$|\Psi_{IM}\rangle = \sum_{K,\kappa} f^I_{K,\kappa} \hat{P}^I_{MK} |\Phi_{N,Z,\kappa}\rangle$$
$$= \sum_{K,\kappa} f^I_{K,\kappa} \frac{2I+1}{8\pi^2} \int d\Omega\, D^{I*}_{MK}(\Omega) \hat{R}(\Omega) |\Phi_{N,Z,\kappa}\rangle, \quad (4)$$

in which the coefficient $f^I_{K,\kappa}$ is determined by the Hill-Wheeler equation,

$$\sum_{K'\kappa'} \left(\langle \Phi_{N,Z,\kappa} | \hat{H} \hat{P}^I_{KK'} | \Phi_{N,Z,\kappa'} \rangle - E_I \langle \Phi_{N,Z,\kappa} | \hat{P}^I_{KK'} | \Phi_{N,Z,\kappa'} \rangle \right) f^I_{K'\kappa'} = 0. \quad (5)$$

It is noted that the information of the orientation of the angular momentum in the intrinsic frame is carried by the quantity K. If one regards $\{K,\kappa\}$ in Eq. (4) as the generator coordinates, the corresponding collective wave-function $g^I(K,\kappa)$ writes [44,45]

$$g^I(K,\kappa) = \sum_{K',\kappa'} \mathcal{N}^{1/2}_I(K,\kappa;K',\kappa') f^I_{K',\kappa'}, \quad (6)$$

with the norm matrix $\mathcal{N}_I(K,\kappa;K',\kappa') \equiv \langle \Phi_{N,Z,\kappa} | \hat{P}^I_{KK'} | \Phi_{N,Z,\kappa'} \rangle$. The K distribution for the angular momentum is as follows:

$$p^I(|K|) = \sum_{\kappa} |g^I(K,\kappa)|^2 + |g^I(-K,\kappa)|^2, \quad (7)$$

which gives the distribution of the long- (l-) axis component of the angular momentum for triaxiality parameter $\gamma \in [0^\circ, 60^\circ]$. The distributions with respect to the short (s) and the intermediate (i) axes are obtained by replacing γ with $\gamma + 120^\circ$ and $\gamma + 240^\circ$ respectively [25].

The angular momentum geometry can also be illustrated by its profile on the (θ,ϕ) plane, *azimuthal plot*, where (θ,ϕ) are the tilted angles of the angular momentum with respect to the intrinsic frame. For $\gamma \in [0^\circ, 60^\circ]$, θ is the angle between the angular momentum and the l axis, whereas ϕ is the angle between the projection of the angular momentum on the i-s plane and the i axis. We found that the profiles can be obtained from the relation between the tilted angles (θ,ϕ) and the Euler angles $\Omega \equiv \{\psi',\theta',\phi'\}$,

$$\theta = \theta', \qquad \phi = \pi - \phi', \quad (8)$$

where the z axis in the laboratory frame is chosen along the angular momentum as illustrated in Fig. 1.

For the eigenfunctions (4), if we choose $\{\Omega,\kappa\}$ as the generator coordinates, the corresponding generating function is $\hat{R}(\Omega)|\Phi_{N,Z,\kappa}\rangle$, and the weight function is $F^{IM}(\Omega,\kappa) \equiv \sum_K f^I_{K,\kappa} \frac{2I+1}{8\pi^2} D^{I*}_{MK}(\Omega)$. The collective wave-function $G^{IM}(\Omega,\kappa)$ is as follows:

$$G^{IM}(\Omega,\kappa) = \sum_{\kappa'} \int d\Omega' \mathcal{M}^{1/2}(\Omega,\kappa;\Omega',\kappa') F^{IM}(\Omega',\kappa')$$
$$= \sqrt{\frac{2I+1}{8\pi^2}} \sum_K g^I(K,\kappa) D^{I*}_{MK}(\Omega), \quad (9)$$

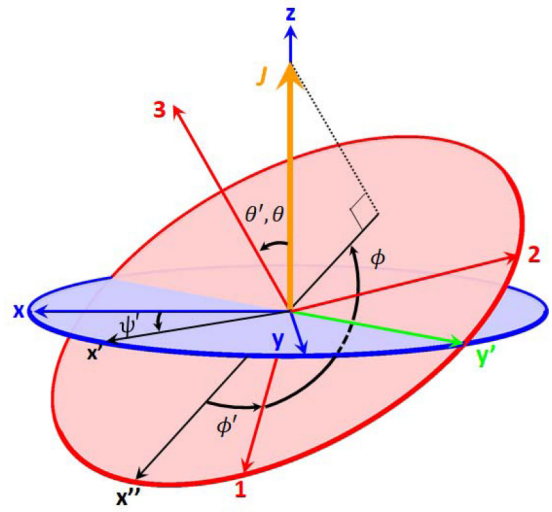

FIG. 1. Illustration of the relation between the tilted angles (θ,ϕ) of the angular momentum with respect to the intrinsic frame (labeled by 1, 2, and 3) and the Euler angles $\{\psi',\theta',\phi'\}$ describing the orientation of the intrinsic frame with respect to the laboratory frame (labeled by x, y, and z).

in which $\mathcal{M}(\Omega,\kappa;\Omega',\kappa') \equiv \langle \Phi_{N,Z,\kappa} | \hat{R}^+(\Omega) \hat{R}(\Omega') | \Phi_{N,Z,\kappa'} \rangle$ and the relation,

$$\mathcal{M}^{1/2}(\Omega,\kappa;\Omega',\kappa') = \sum_{IM} \sum_{KK'} \sqrt{\frac{2I+1}{8\pi^2}} \mathcal{N}^{1/2}_I(K,\kappa;K',\kappa') \times D^{I*}_{MK}(\Omega) D^I_{MK'}(\Omega'), \quad (10)$$

has been used.

Therefore, the *azimuthal plot*, i.e., the profile for the orientation of the angular momentum on the (θ,ϕ) plane writes

$$\mathcal{P}(\theta,\phi) = \sum_{\kappa} \int_0^{2\pi} d\psi' |G^{II}(\psi',\theta,\pi-\phi,\kappa)|^2. \quad (11)$$

In the following, the doublet bands in ^{128}Cs [14] are investigated as an example by the AMP approach. The parameters in the Hamiltonian (1) are taken from Ref. [40]. In the calculation, the quadrupole deformation parameters (β,γ) are constrained to be $(0.20, 30.0^\circ)$. This choice of (β,γ) is close to the ground-state deformation $(0.23, 23.8^\circ)$ [46] given by the covariant density-functional theory (CDFT) [47–50] with interaction PC-PK1 [51]. It agrees reasonably with the deformations $(0.20, 37.0^\circ)$ used in the projected shell-model calculation [40]. The yrast band is obtained by blocking the lowest $\pi h_{11/2}$ and the fourth $\nu h_{11/2}$ orbitals, which is consistent with the CDFT results [46].

The calculated energy spectra, the intraband $B(E2)$ and $B(M1)$, and the interband $B(M1)$ of the doublet bands (denoted as band A and band B, respectively) in ^{128}Cs are shown in Fig. 2 in comparison with the available data [14].

The observed energy spectra are reproduced excellently as shown in Fig. 2(a), including the energy difference between the partner bands.

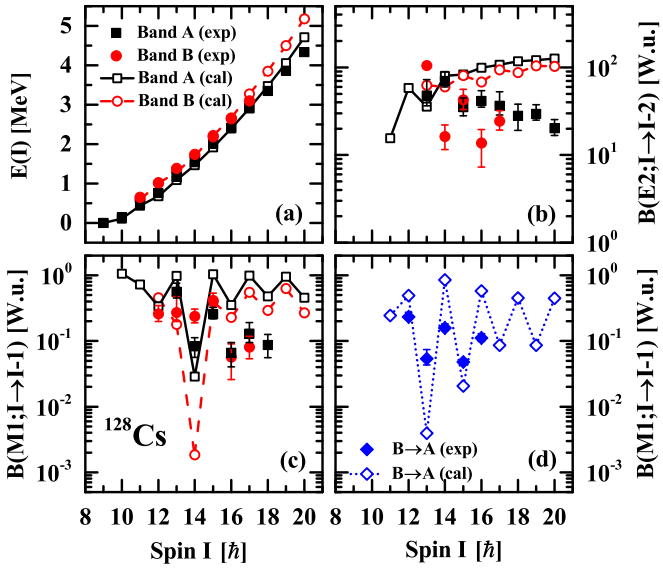

FIG. 2. (a) The energy spectra, (b) the intraband $B(E2)$, (c) $B(M1)$, and (d) the interband $B(M1)$ of the doublet bands in ^{128}Cs calculated by the AMP approach in comparison with the data available [14].

The similarity of $B(E2)$ between bands A and B, which qualified ^{128}Cs as the best example of a chiral nucleus, is found in both the data and the calculated results as shown in Fig. 2(b). The strength of the calculated $B(E2)$ agrees with the data near the bandhead. With the increasing spin, the trend of the calculated results deviates from the data due to the frozen nuclear shape. The quality of agreement is comparable with that of the core-quasiparticle coupling model [14,52].

The staggering of the intra- and the interband $B(M1)$, another signature of chiral modes [23,53], can be seen in both the data and the calculated results as shown in Figs. 2(c) and 2(d).

As the main features of the chiral bands in ^{128}Cs [14] are well reproduced by the present calculation, it is interesting to study the evolution of the angular momentum geometry and its chiral geometry.

In Fig. 3, the *K plot*, i.e., the calculated K-distribution $p^I(|K|)$ (7) for the doublet bands in ^{128}Cs, is shown for $I =$ 11, 14, and 18$\hbar$. A similar discussion has been conducted extensively within the framework of the PRM [25,54]. As seen in the figure, the evolution of the chiral modes from the chiral vibration near the bandhead to the static chirality at higher spins is exhibited.

For $I = 11\hbar$, the probability at $K_i = 0$ is significant for band A, whereas it vanishes for band B. This is in accordance with the interpretation of the chiral vibration with respect to the s-l plane where the zero-phonon state (band A) is symmetric with respect to $K_i = 0$ and the one-phonon state (band B) is antisymmetric [25,54].

For $I = 14\hbar$, the maximum probability for K_i appears at $K_i \sim 12\hbar$ for band A, which means, with the increase in spin, the orientation of the angular momentum deviates from the s-l plane and aplanar rotation occurs. The K distributions of band B are similar to those of band A, which indicates the appearance of static chirality. The finite values of $p(K_i = 0)$ and $p(K_l = 0)$ reflect the tunneling between the left-handed

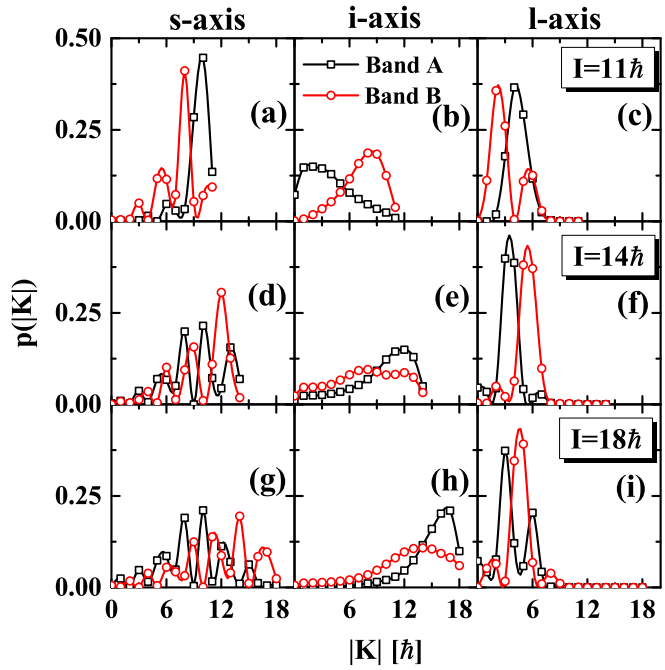

FIG. 3. The *K plot*, i.e., K distributions for the angular momentum on the short (s), intermediate (i), and long (l) axes, calculated at $I = 11$ (a)–(c), 14 (d)–(f), and 18$\hbar$ (g)–(i), respectively.

and the right-handed configurations, which is responsible for the energy difference remaining between bands A and B.

For $I = 18\hbar$, the energy difference between the chiral partners increases, and the similarity between the K distributions of the two bands becomes less pronounced, which weakens the feature of static chirality.

In Fig. 4, the *azimuthal plot*s, i.e., the profiles $\mathcal{P}(\theta,\phi)$ of the doublet bands in ^{128}Cs are shown for $I = 11, 14$, and 18$\hbar$ in order to examine the orientation of the angular momentum on the (θ,ϕ) plane.

For $I = 11\hbar$, the angular momentum for band A mainly orientates at ($\theta \sim 60^\circ$, $\phi = 90^\circ$), namely, a planar rotation within the s-l plane. The angular momentum for band B

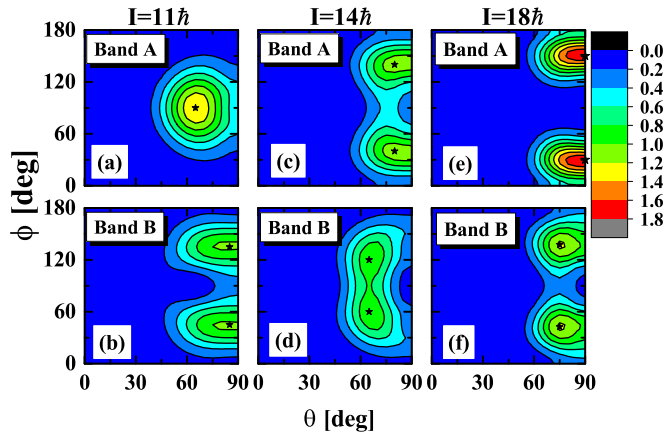

FIG. 4. The *azimuthal plot*, i.e., profile for the orientation of the angular momentum on the (θ,ϕ) plane, calculated at $I = 11$ [(a), (b)], 14 [(c), (d)], and 18$\hbar$ [(e), (f)], respectively.

orientates equally at ($\theta \sim 85°$, $\phi \sim 45°$) and ($\theta \sim 85°$, $\phi \sim 135°$), in accordance with the interpretation of chiral vibration along the ϕ direction (i.e., with respect to the s-l plane). Here, $\theta \sim 85°$ means that the angular momentum is located very close to the i-s plane, which is consistent with the K_l distribution shown in Fig. 3(c), the peak at $K_l = 2\hbar$.

For $I = 14\hbar$, the angular momenta orientate equally at two directions for bands A [($\theta \sim 80°$, $\phi \sim 40°$) and ($\theta \sim 80°$, $\phi \sim 140°$)] and B [($\theta \sim 65°$, $\phi \sim 60°$) and ($\theta \sim 65°$, $\phi \sim 120°$)], which demonstrates the occurrence of static chirality. The tunneling between the left-handed and the right-handed configurations is reflected by the nonvanishing probability for either $\phi = 90°$ or $\theta = 90°$ as well as the fact that the orientations of the angular momenta of band A do not coincide exactly with those of band B.

For $I = 18\hbar$, the static chirality disappears. The angular momenta for band A orientate to ($\theta = 90°$, $\phi = 30°$) and ($\theta = 90°$, $\phi = 150°$), corresponding to a planar rotation within the i-s plane. The angular momenta for band B orientate at ($\theta = 75°$, $\phi = 45°$) and ($\theta = 75°$, $\phi = 135°$) due to quantum fluctuation. The profiles here are in accordance with the conclusion obtained from the *K plot*.

From Figs. 3 and 4, the chiral geometry in the symmetry-restored states is illustrated by the *K plot* and the *azimuthal plot*.

To summarize, the chiral modes are investigated with the AMP approach by diagonalizing the pairing-plus-quadrupole Hamiltonian in a symmetry-restored basis. The chiral features in ^{128}Cs [14], including the near degeneracy between the partner bands, the similarity of $B(E2)$, and the staggering of $B(M1)$, are reproduced without any free parameters. To provide the chiral picture from the AMP description, the chiral geometry in the intrinsic frame is examined. The challenge to extract the chiral geometry of the angular momentum in the AMP approach is overcome by treating the components of the angular momentum in the intrinsic frame and the Euler angles, respectively, as generator coordinates. The K distribution in the intrinsic frame (*K plot*) and the profile $\mathcal{P}(\theta,\phi)$ for the orientation of the angular momentum (*azimuthal plot*) are obtained, and the chiral geometry in the symmetry-restored states is illustrated. It should be noted that the AMP approach for chiral modes here can be generalized and combined with the state-of-art mean-field approaches [50]. Applications for other exotic rotational modes, such as the wobbling mode [55], are also possible.

We thank Z. C. Gao for his help and discussion in the implementation of the computing codes and X. H. Wu for his help in preparing Fig. 1. Stimulating discussions with Z. C. Gao, F. Pan, Y. Sun, S. Y. Wang, and other participants in the workshop "Nuclear spontaneous symmetry breaking and its experimental signals" are acknowledged. This work was partly supported by the Chinese Major State 973 Program No. 2013CB834400, the National Natural Science Foundation of China (Grants No. 11335002, No. 11375015, No. 11461141002, and No. 11621131001), and the China Postdoctoral Science Foundation under Grants No. 2015M580007, No. 2016T90007 and No. 2017M610688.

[1] S. Frauendorf and J. Meng, Nucl. Phys. A **617**, 131 (1997).
[2] K. Starosta, T. Koike, C. J. Chiara, D. B. Fossan, D. R. LaFosse, A. A. Hecht, C. W. Beausang, M. A. Caprio, J. R. Cooper, R. Krücken *et al.*, Phys. Rev. Lett. **86**, 971 (2001).
[3] S. Y. Wang, B. Qi, L. Liu, S. Q. Zhang, H. Hua, X. Q. Li, Y. Y. Chen, L. H. Zhu, J. Meng, S. M. Wyngaardt *et al.*, Phys. Lett. B **703**, 40 (2011).
[4] C. Liu, S. Y. Wang, R. A. Bark, S. Q. Zhang, J. Meng, B. Qi, P. Jones, S. M. Wyngaardt, J. Zhao, C. Xu *et al.*, Phys. Rev. Lett. **116**, 112501 (2016).
[5] C. Vaman, D. B. Fossan, T. Koike, K. Starosta, I. Y. Lee, and A. O. Macchiavelli, Phys. Rev. Lett. **92**, 032501 (2004).
[6] P. Joshi, M. P. Carpenter, D. B. Fossan, T. Koike, E. S. Paul, G. Rainovski, K. Starosta, C. Vaman, and R. Wadsworth, Phys. Rev. Lett. **98**, 102501 (2007).
[7] D. Tonev, M. S. Yavahchova, N. Goutev, G. de Angelis, P. Petkov, R. K. Bhowmik, R. P. Singh, S. Muralithar, N. Madhavan, R. Kumar *et al.*, Phys. Rev. Lett. **112**, 052501 (2014).
[8] E. O. Lieder, R. M. Lieder, R. A. Bark, Q. B. Chen, S. Q. Zhang, J. Meng, E. A. Lawrie, J. J. Lawrie, S. P. Bvumbi, N. Y. Kheswa *et al.*, Phys. Rev. Lett. **112**, 202502 (2014).
[9] N. Rather, P. Datta, S. Chattopadhyay, S. Rajbanshi, A. Goswami, G. H. Bhat, J. A. Sheikh, S. Roy, R. Palit, S. Pal *et al.*, Phys. Rev. Lett. **112**, 202503 (2014).
[10] I. Kuti, Q. B. Chen, J. Timár, D. Sohler, S. Q. Zhang, Z. H. Zhang, P. W. Zhao, J. Meng, K. Starosta, T. Koike *et al.*, Phys. Rev. Lett. **113**, 032501 (2014).
[11] S. Zhu, U. Garg, B. K. Nayak, S. S. Ghugre, N. S. Pattabiraman, D. B. Fossan, T. Koike, K. Starosta, C. Vaman, R. V. F. Janssens *et al.*, Phys. Rev. Lett. **91**, 132501 (2003).
[12] D. Tonev, G. de Angelis, P. Petkov, A. Dewald, S. Brant, S. Frauendorf, D. L. Balabanski, P. Pejovic, D. Bazzacco, P. Bednarczyk *et al.*, Phys. Rev. Lett. **96**, 052501 (2006).
[13] C. M. Petrache, G. B. Hagemann, I. Hamamoto, and K. Starosta, Phys. Rev. Lett. **96**, 112502 (2006).
[14] E. Grodner, J. Srebrny, A. A. Pasternak, I. Zalewska, T. Morek, C. Droste, J. Mierzejewski, M. Kowalczyk, J. Kownacki, M. Kisieliński *et al.*, Phys. Rev. Lett. **97**, 172501 (2006).
[15] S. Mukhopadhyay, D. Almehed, U. Garg, S. Frauendorf, T. Li, P. V. M. Rao, X. Wang, S. S. Ghugre, M. P. Carpenter, S. Gros *et al.*, Phys. Rev. Lett. **99**, 172501 (2007).
[16] A. D. Ayangeakaa, U. Garg, M. D. Anthony, S. Frauendorf, J. T. Matta, B. K. Nayak, D. Patel, Q. B. Chen, S. Q. Zhang, P. W. Zhao *et al.*, Phys. Rev. Lett. **110**, 172504 (2013).
[17] D. L. Balabanski, M. Danchev, D. J. Hartley, L. L. Riedinger, O. Zeidan, J.-y. Zhang, C. J. Barton, C. W. Beausang, M. A. Caprio, R. F. Casten *et al.*, Phys. Rev. C **70**, 044305 (2004).
[18] E. A. Lawrie, P. A. Vymers, J. J. Lawrie, C. Vieu, R. A. Bark, R. Lindsay, G. K. Mabala, S. M. Maliage, P. L. Masiteng, S. M. Mullins *et al.*, Phys. Rev. C **78**, 021305 (2008).
[19] J. Meng and S. Q. Zhang, J. Phys. G: Nucl. Part. Phys. **37**, 064025 (2010).
[20] J. Meng, Q. B. Chen, and S. Q. Zhang, Int. J. Mod. Phys. E **23**, 1430016 (2014).

[21] J. Meng and P. W. Zhao, Phys. Scr. **91**, 5 (2016).
[22] J. Peng, J. Meng, and S. Q. Zhang, Phys. Rev. C **68**, 044324 (2003).
[23] T. Koike, K. Starosta, and I. Hamamoto, Phys. Rev. Lett. **93**, 172502 (2004).
[24] S. Q. Zhang, B. Qi, S. Y. Wang, and J. Meng, Phys. Rev. C **75**, 044307 (2007).
[25] B. Qi, S. Q. Zhang, J. Meng, S. Y. Wang, and S. Frauendorf, Phys. Lett. B **675**, 175 (2009).
[26] V. I. Dimitrov, S. Frauendorf, and F. Dönau, Phys. Rev. Lett. **84**, 5732 (2000).
[27] H. Madokoro, J. Meng, M. Matsuzaki, and S. Yamaji, Phys. Rev. C **62**, 061301 (2000).
[28] P. Olbratowski, J. Dobaczewski, J. Dudek, and W. Płóciennik, Phys. Rev. Lett. **93**, 052501 (2004).
[29] P. Olbratowski, J. Dobaczewski, and J. Dudek, Phys. Rev. C **73**, 054308 (2006).
[30] P. W. Zhao, Phys. Lett. B **773**, 1 (2017).
[31] D. Almehed, F. Dönau, and S. Frauendorf, Phys. Rev. C **83**, 054308 (2011).
[32] Q. B. Chen, S. Q. Zhang, P. W. Zhao, R. V. Jolos, and J. Meng, Phys. Rev. C **87**, 024314 (2013).
[33] Q. B. Chen, S. Q. Zhang, P. W. Zhao, R. V. Jolos, and J. Meng, Phys. Rev. C **94**, 044301 (2016).
[34] D. Tonev, G. de Angelis, S. Brant, S. Frauendorf, P. Petkov, A. Dewald, F. Dönau, D. L. Balabanski, Q. Zhong, P. Pejovic *et al.*, Phys. Rev. C **76**, 044313 (2007).
[35] S. Brant, D. Tonev, G. de Angelis, and A. Ventura, Phys. Rev. C **78**, 034301 (2008).
[36] K. Hara and Y. Sun, Int. J. Mod. Phys. E **04**, 637 (1995).
[37] Y. Sun and D. H. Feng, Phys. Rep. **264**, 375 (1996).
[38] J. A. Sheikh and K. Hara, Phys. Rev. Lett. **82**, 3968 (1999).
[39] Y. Sun, Phys. Scr. **91**, 043005 (2016).
[40] Z. C. Gao, Y. Chen, and Y. Sun, Phys. Lett. B **634**, 195 (2006).
[41] J. A. Sheikh, G. H. Bhat, Y. Sun, G. B. Vakil, and R. Palit, Phys. Rev. C **77**, 034313 (2008).
[42] G. H. Bhat, J. A. Sheikh, and R. Palit, Phys. Lett. B **707**, 250 (2012).
[43] G. H. Bhat, R. N. Ali, J. A. Sheikh, and R. Palit, Nucl. Phys. A **922**, 150 (2014).
[44] P. Ring and P. Schuck, *The Nuclear Many Body Problem* (Springer-Verlag, Berlin, 1980).
[45] F. Q. Chen and J. L. Egido, Phys. Rev. C **95**, 024307 (2017).
[46] E. Grodner *et al.* (unpublished).
[47] P. Ring, Prog. Part. Nucl. Phys. **37**, 193 (1996).
[48] D. Vretenar, A. V. Afanasjev, G. A. Lalazissis, and P. Ring, Phys. Rep. **409**, 101 (2005).
[49] J. Meng, H. Toki, S. G. Zhou, S. Q. Zhang, W. H. Long, and L. S. Geng, Prog. Part. Nucl. Phys. **57**, 470 (2006).
[50] J. Meng (ed.), *Relativistic Energy Density Functional for Nuclear Structure*, International Review of Nuclear Physics Vol. 10 (World Scientific, Singapore, 2016).
[51] P. W. Zhao, Z. P. Li, J. M. Yao, and J. Meng, Phys. Rev. C **82**, 054319 (2010).
[52] T. Koike, K. Starosta, C. J. Chiara, D. B. Fossan, and D. R. LaFosse, Phys. Rev. C **67**, 044319 (2003).
[53] S. Y. Wang, S. Q. Zhang, B. Qi, and J. Meng, Chin. Phys. Lett. **24**, 664 (2007).
[54] B. Qi, S. Q. Zhang, S. Y. Wang, J. M. Yao, and J. Meng, Phys. Rev. C **79**, 041302(R) (2009).
[55] A. Bohr and B. R. Mottelson, *Nuclear Structure* (Benjamin, New York, 1975).